PCCP

Collisional dynamics simulations revealing fragmentation properties of Zn(II)-bound poly-peptide

Journal:	*Physical Chemistry Chemical Physics*
Manuscript ID	CP-ART-05-2020-002463.R1
Article Type:	Paper
Date Submitted by the Author:	19-Jun-2020
Complete List of Authors:	Malik, Abdul; Texas Tech University, Chemistry and Biochemistry angel, laurence; Texas A&M University Commerce, Chemistry Spezia, Riccardo; Sorbonne Université, Laboratoire de Chimie Théorique UMR 7616 Hase, William; Texas Tech University, Depart of Chemistry and Biochemistry

PCCP

RSCPublishing

ARTICLE

Collisional dynamics simulations revealing fragmentation properties of Zn(II)-bound poly-peptide

Received 00th April 20xx,
Accepted 00th April 20xx

DOI: 10.1039/x0xx00000x

Abdul Malik,[a] Laurence A. Angel,[b] Riccardo Spezia[c],* and William L. Hase[a]

Chemical dynamics simulations are performed to study the collision induced gas phase unimolecular fragmentation of a model peptide with the sequence acetyl-His_1-Cys_2-Gly_3-Pro_4-Tyr_5-His_6-Cys_7 (analogue methanobactin peptide-5, amb_5) and in particular to explore the role of zinc binding on reactivity. Fragmentation pathways, their mechanisms, and collision energy transfer are discussed. The probability distributions of the pathways are compared with the results of the experimental IM-MS, MS/MS spectrum and previous thermal simulations. Collisional activation gives both statistical and non-statistical fragmentation pathways with non-statistical shattering mechanisms accounting for a relevant percentage of reactive trajectories, becoming dominant at higher energies. The tetra-coordination of zinc changes qualitative and quantitative fragmentation, in particular the shattering. The collision energy threshold for the shattering mechanism was found to be 118.9 kcal/mol which is substantially higher than the statistical Arrhenius activation barrier of 35.8 kcal/mol identified previously during thermal simulations. This difference can be attributed to the tetra-coordinated zinc complex that hinders the availability of the sidechains to undergo direct collision with the Ar projectile.

Introduction

Zinc plays an important role in biological systems[1] where it can either aid in catalysis or provide structural support to maintain the protein conformation.[2] These functions are performed by incorporating zinc as a cofactor into proteins or peptides usually via thiolate groups of cysteine and the imidazole groups of histidine in a distorted tetrahedral coordination geometry.[3–7] For example, matrix metalloproteinases are zinc-dependent enzymes that catalyze the hydrolysis of structural proteins in the extracellular matrix[8] and their inhibition has been investigated for slowing the progression of cancers.[9] The eukaryotic zinc finger proteins have conformations that are specific for binding to DNA[10,11] and the zinc ion is most commonly tetrahedrally coordinated via 2Cys-2His.[2,11–13]

Ion mobility - mass spectrometry (IM-MS)[6,14,15] with molecular modelling and novel ion activation methods can be used to determine the accurate structure of these zinc containing metallopeptides. Previous studies of methanobactin[16,17] from *Methylosinus trichosporium* and analogue methanobactin (amb) peptides[6,14,15,18–21] show the IM-MS analyses in negative ion mode is particularly informative because it shows a distinct pH dependence for the metal binding and provides the protonation state of the acidic and basic binding sites, the charge of the metal ion, and the collision cross section of the conformer. The primary structures of the amb peptides include Pro as a hinge to position the His and Cys substituent groups for coordinating the metal ion (Figure 1).

After decades of development, collisional activation is still one of the most popular activation methods and is routinely used in peptide science.[22] Collision induced dissociation (CID) involves energetic collisions between ions and neutral gas atoms which result in the transfer of translational energy to the internal energy of the ion.[23] This excess ro-vibrational energy causes dissociation of the precursor ion and generates product ions which are mass analyzed (the so-called MS/MS).

Theoretical mass spectrometry, in the form of direct dynamics simulations,[24,25] combined with experimental IM-MS and MS/MS can be used to obtain atomistic level information about biomolecules. The dissociation pathways and products found through experimental and theoretical studies can be used to illuminate the main fragmentation features of the peptides. Due to their high efficiency, collisional activation methods are routinely used in most of the tandem mass spectrometry instruments (ion traps, Fourier-transform ion cyclotron resonance, quadrupole time-of-flight, etc.).[26–29] There are certain details in the CID fragmentation mechanisms that are still of interest including the role of the side chains,[30–34] or the effect of the collisional activation mode on the fragmentation products.[35] Theoretical simulations can be used to answer these queries.[25,36,37] There are two main activation methods employed in chemical dynamics simulations of biomolecules. One involves thermal (internal energy) excitation to reflect multiple collisions and the other is the single collision excitation with an inert gas molecule.[24,25]

[a] *Department of Chemistry and Biochemistry, Texas Tech University, Lubbock, Texas 79409-1061 USA*
[b] *Department of Chemistry, Texas A&M University-Commerce, 2600 S Neal Street, Commerce, TX, 75428, USA*
[c] *Laboratoire de Chimie Théorique, Sorbonne Université, UMR 7616 CNRS, 4, Place Jussieu, 75005 Paris, France*
* *correspondence to: riccardo.spezia@sorbonne-universite.fr*
Electronic Supplementary Information (ESI) available: [details of any supplementary information available should be included here]. See DOI: 10.1039/x0xx00000x

In experimental MS/MS spectra, product ions due to both statistical and non-statistical mechanisms appear but their ratio depends on the experimental conditions.[38] For example, fragmentation occurring in tandem mass spectrometers and extrapolated to the single collision CID can provide reaction cross sections as a function center-of-mass collision energy.[39] Simulations of single collision CID can be useful to understand fragmentation mechanisms of peptides.[22,37,40] For the fragment dissociation of large molecules, efficient energy transfer during the collision is required.[41] Similarly to what was recognized by the previous studies on surface-induced dissociation (SID)[42–47] the dynamics for the ions excited by this CID mode experience key differences with respect to randomized unimolecular fragmentation,[45] which relies on the well-known Rice–Ramsperger–Kassel–Marcus (RRKM) theory.[48] This theory is based on statistical assumption requiring that translation to vibration energy transfer during the collision occurs within intramolecular vibrational energy redistribution (IVR). For these non-random dynamics, the decay of the initial population will be non-exponential, as recently shown in the case of di-proline anion CID simulations.[38] One relevant non-statistical mechanism observed in CID is the so-called shattering:[49,50] the collision activates one (or more) vibrational mode(s), leading to fragmentation within one vibrational period of the bond which breaks. Shattering fragmentation during CID has been observed in previous chemical dynamics simulations and experiments for protonated urea,[49,51] protonated uracil,[52,53] CH_3SH^+,[54,55] and $Cr^+(CO)_6$[56] and more recently in polypeptides.[36–38,57,58] To have a better estimate of the expected ions from an excitation method during experimental mass spectrometry, it is important to compare fragmentation pathways and product ions for different excitation methods using direct dynamics simulations.

Direct chemical dynamics simulations[59,60] were recently[61] used to analyse fragmentation of thermally excited $[amb_5–3H+Zn(II)]^-$ and can be now used to study non-random CID fragmentation as has been used in the past to analyse e.g. protonated poly-glycines,[57,58] and a di-proline anion[38] and $TIK(H^+)_2$.[36,37] During thermal excitation,[61] $[amb_5–3H+Zn(II)]^-$ ion was excited at temperatures ranging from 1600 to 2250 K and the energy was randomly distributed in the vibrational modes of the ion. The kinetic analysis showed that fragmentation probability of $[amb_5–3H+Zn(II)]^-$ follows RRKM theory. Out of the three lowest energy conformers of $[amb_5–3H+Zn(II)]^-$, that were thermally excited in ref. 51, chemical dynamics simulations are here performed on conformer *a* (structure shown in Figure 1) since its fragmentation pattern most closely matched with the experiment. We now investigate how the same peptide will fragment under explicit collision simulations with Ar. In this case, the ion will be excited non-randomly and the site of collision will have a major impact on fragmentation dynamics. Differently to peptides studied previously via CID, the one reported here is the first presenting a tetra-coordination binding to a transition metal. This could result in substantial differences. To have a more detailed picture of the effects of explicit collision, we compared the results reported here with those obtained in the previously reported study under thermal excitation conditions.[61]

Computational Methodology

Electronic Structure Theory. Previous simulations[61] of the thermal fragmentation of $[amb_5–3H+Zn(II)]^-$ used PM7,[62] semi-empirical electronic structure theory method. In this same previous work, the PM7 method was shown to be able to correctly describe the reactivity of this system. We have thus employed PM7 in the present work. Here, PM7 was used also to describe the interaction between the peptide and Ar atom. With respect to previous semi-empirical Hamiltonians of the same family, PM7 implicitly addresses dispersion by including non-covalent systems in the training set during the parameterization and is thus able to describe also Ar, for which parameters are reported in the litteraure.[62] As initial structure of the ion for subsequent collisional dynamics simulation, we used the lowest energy structure of the peptide found previously,[61] notably conformer *a*.

Direct Dynamics Simulations. $[amb_5–3H+Zn(II)]^-$ collisional direct dynamics simulations were performed with a VENUS/MOPAC software package which consists of an interface between the VENUS[63] chemical dynamics computer program and the MOPAC[64] electronic structure theory computer program.

Quasi-classical initial conditions[65] were selected for the ion, with its initial vibrational energies chosen from 300 K normal mode Boltzmann distribution. For rotational energy, a classical Boltzmann sampling at 300K was used. To set the collisional system (ion + Ar), the ion was randomly rotated about its Euler angles. The initial distance between the ion and Ar was set at 15 Å, in order to have no initial interaction between the ion and the neutral projectile. The impact parameter was randomly chosen between 0 to 9.5 Å. This maximum value was chosen on geometrical consideration: the maximum radius of the ion is about 8.8 Å and thus at 9.5 Å no noticeable interactions occur.

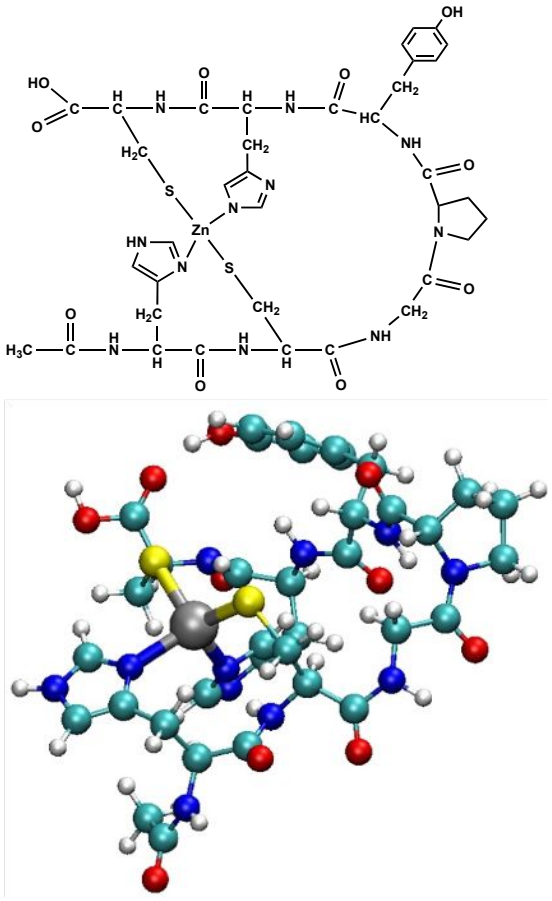

Figure 1. Schematic diagram of conformer *a* of $[amb_5–3H+Zn(II)]^-$ and 3D structure of its optimized geometry. grey, Zn; yellow, S; cyan; C, blue, N; red, O; white, H.

Collisional simulations were performed for relative translational energies (E_{rel}) of 10.8, 13.0, 26.0 and 39.0 eV between Ar and $[amb_5–3H+Zn(II)]^-$. These values were chosen in order to have increasing fragmentation yields. In fact, 10.8 eV is the lowest energy for which

PCCP RSCPublishing

ARTICLE

Table 1. Fragmentation pathways, probabilities of total reactive trajectories, and probability that the pathway followed a shattering mechanism for E_{rel} = 10.8, 13, 26, and 39 eV. In parentheses is the probability that the pathway followed a shattering mechanism.

			Probability[a] for E_{rel} (eV)			
Pathway	*m/z*	Dissociation Site	10.8	13	26	39
1	766.1	Backbone	21.0 ± 5.2 (7.7 ± 5.7)	7.6 ± 1.8 (37.5 ± 4.3)	6.7 ± 1.9 (41.7 ± 4.4)	4.7 ± 1.4 (63.6 ± 3.4)
2	873.2	Backbone	12.9 ± 4.3 (37.5 ± 10.3)	5.7 ± 1.6 (58.3 ± 4.4)	4.5 ± 1.6 (75.0 ± 3.9)	4.7 ± 1.4 (54.5 ± 3.7)
3	837.2	Sidechain	6.5 ± 3.1 (75.0 ± 9.2)	3.3 ± 1.2 (57.1 ± 4.4)	5.1 ± 1.6 (77.8 ± 3.7)	5.2 ± 1.4 (100.0)
4	890.2	Backbone	8.1 ± 3.5 (40.0 ± 10.4)	6.6 ± 1.7 (78.6 ± 3.7)	6.2 ± 1.8 (90.9 ± 2.6)	4.3 ± 1.3 (90.0 ± 2.1)
5	723.1	Backbone	6.5 ± 3.1 (50.0 ± 10.7)	0.9 ± 0.7 (50.0 ± 4.5)	4.5 ± 1.6 (75.0 ± 3.9)	-
6	821.2	Backbone	3.2 ± 2.2 (0.0)	2.4 ± 1.0 (20.0 ± 3.6)	1.7 ± 1.0 (0.0)	3.4 ± 1.2 (87.5 ± 2.4)
7	875.2	Backbone	3.2 ± 2.2 (0.0)	3.3 ± 1.2 (42.9 ± 4.4)	4.5 ± 1.6 (75.0 ± 3.9)	5.2 ± 1.4 (91.7 ± 2.0)
8	860.2	Backbone	3.2 ± 2.2 (50.0 ± 10.7)	4.7 ± 1.5 (90.0 ± 2.7)	1.1 ± 0.8 (100.0)	-
9	738.1	Backbone	1.6 ± 1.6 (100.0)	1.4 ± 0.8 (33.3 ± 4.2)	2.8 ± 1.2 (40.0 ± 4.4)	3.0 ± 1.1 (85.7 ± 2.5)
10	696.1	Backbone	3.2 ± 2.2 (0.0)	3.3 ± 1.2 (28.6 ± 4.1)	1.1 ± 0.8 (0.0)	-
11	811.2	Sidechain	-	6.2 ± 1.7 (84.6 ± 3.2)	2.2 ± 1.1 (100.0)	3.0 ± 1.1 (85.7 ± 2.5)
12	636.1	Backbone	1.6 ± 1.6 (0.0)	0.5 ± 0.5 (0.0)	-	0.4 ± 0.4 (100.0)
13	903.2	Backbone	-	5.2 ± 1.5 (100.0)	3.4 ± 1.4 (100.0)	1.3 ± 0.7 (100.0)
14	872.2	Sidechain	-	1.9 ± 0.9 (100.0)	1.7 ± 1.0 (66.7 ± 4.3)	0.9 ± 0.6 (100.0)
15	849.1	Backbone	-	0.5 ± 0.5 (0.0)	1.1 ± 0.8 (0.0)	1.3 ± 0.7 (100.0)
16	885.2	Sidechain	-	0.5 ± 0.5 (0.0)	0.6 ± 0.6 (0.0)	0.4 ± 0.4 (0.0)
17	771.2	Backbone	-	1.4 ± 0.8 (66.7 ± 4.2)	0.6 ± 0.6 (0.0)	2.6 ± 1.0 (66.7 ± 3.4)
18	845.2	Backbone	-	1.9 ± 0.9 (25.0 ± 3.9)	-	0.9 ± 0.6 (50.0 ± 3.6)
19	889.2	Sidechain		1.4 ± 0.8 (33.3 ± 4.2)	0.6 ± 0.6 (100.0)	0.4 ± 0.4 (100.0)
20	840.2	Backbone	1.6 ± 1.6 (0.0)	1.4 ± 0.8 (0.0)	-	-
21	917.2	H atom	3.2 ± 2.2 (100.0)	8.1 ± 1.9 (100.0)	14.6 ± 2.6 (100.0)	15.9 ± 2.4 (100.0)
22	916.2	H_2 molecule	1.6 ± 1.6 (100.0)	1.9 ± 0.9 (100.0)	3.4 ± 1.4 (100.0)	4.7 ± 1.4 (100.0)
23	901.2	Sidechain	3.2 ± 2.2 (0.0)	1.9 ± 0.9 (100.0)	3.4 ± 1.4 (100.0)	-
Other			21.0 ± 5.2 (30.8 ± 9.8)	27.0 ± 3.1 (42.4 ± 4.4)	30.3 ± 3.4 (51.9 ± 4.5)	38.2 ± 3.2 (80.9 ± 2.8)

[a] The percentage probability of this pathway against the total reactive trajectories. [b] Percentage probability of all the other pathways with respect to the reactive trajectories. The uncertainties are the standard deviations of the percentages.

some fragmentation is observed. The higher collision energies are chosen to get a clear energy dependent picture of shattering as well as non-shattering mechanisms. Once a fragmentation occurs, Mulliken population analysis was performed on the atoms of the system at the final geometry and charge localized on one fragment. The total spin of the system was conserved (and singlet) in all calculations. Finally, a trajectory is considered as shattering if the fragmentation occurs in less than 40 fs after the collision, which is an arbitrary limit assuming that the bond dissociation occurs within this time period before IVR could take place. (similar time limit was used in a previous study[37]). 2000 trajectories were run each for 10.8 and 13 eV, and 1000 trajectories each for 26 and 39 eV. For all the collision energies, trajectories were integrated up to 20 ps.

Simulation Results

Primary Dissociation Pathways. The dissociation dynamics of $[amb_5–3H+Zn(II)]^-$ subsequent to collision with Ar projectile are discussed here in detail. In particular, we first report in Table 1 the probabilities (as percentage over the total reactive trajectories) of the most abundant primary dissociation pathways (23), specifying if the fragmentation occurs on the backbone or the sidechain. The nomenclature[66] used previously[61] to represent peptide fragments in mass spectrometry is employed here and is shown in Figure 2 for analogue methanobactin peptide-5, amb_5. In Table 1 (in parentheses) the probability that the pathway follows a shattering mechanism is also specified. Pathways 1-20 are shown in the supporting information in Figure S1. Pathways 21-23 correspond to the loss of H, H_2, and OH.

As expected, the number of open pathways increases as the collision energy increases: they are 22, 59, 60 and 63 for 10.8, 13, 26 and 39 eV collision energy, respectively. Also, the percentage of the reactive trajectories increases with the collision energy: there are 6.2, 12.8, 20.9, and 23.3 percent reactive trajectories for E_{rel} of 10.8, 13, 26, and 39 eV, respectively. Some trajectories involve a H atom transfer

PCCP RSCPublishing

ARTICLE

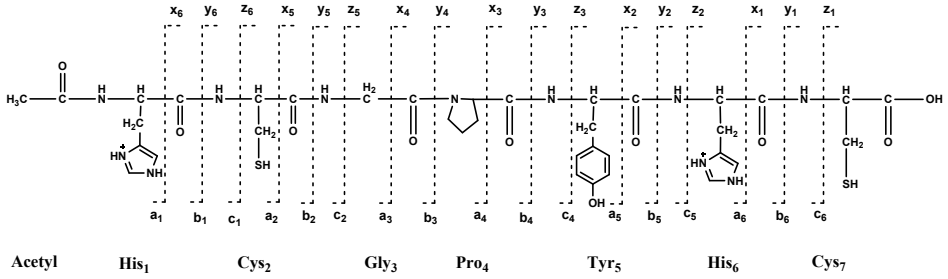

Figure 2. Primary structure of amb$_5$ without Zn(II) and abbreviation used to characterize the fragments.[66]

following a bond dissociation; however, the tetra-coordinated nature of the zinc complex implies that a single bond dissociation may not result in formation of two or more fragments. Such trajectories are characterized as non-reactive, at least in the time-length available from our simulations. For example, for E_{rel} = 13 eV 2.2 % of the total trajectories resulted in a H atom transfer that did not lead to fragmentation. H atoms most susceptible to be transferred are the ones bonded to either oxygen or nitrogen and they are most likely to be transferred to either of the thiol groups following the breaking of Zn-S bond.

Pathway 1 resulting in *m/z* 766.1 product ion for $[x_6+Zn(II)]^-$ was the most frequent pathway for E_{rel} = 10.8 eV (lowest collision energy considered) and the second most abundant following pathway 21, which was the loss of H atom, at all three higher collision energies. Pathway 2 with product ion *m/z* 873.2 was observed due to the loss of terminal COOH molecule, at four collision energies, which also had a coincidental mass loss with two other distinct fragmentation mechanisms. For example, at E_{rel} = 10.8, 13, and 26 eV it was found for the loss of (CO_2+H) and at 13 eV the loss of (CO+OH) gave the same *m/z* final ion product. Pathway 3 with *m/z* 837.2 for product ion with the loss of (CH_2+imi) was observed at all four collision energies almost exclusively due to shattering. Pathway 4, *m/z* 890.2 for the loss of CO molecule, was seen for all E_{rel}. Pathway 5, resulting in product ion *m/z* 723.1 for the fragment $[z_6+Zn(II)]^-$, was observed only for collision energies of 10.8, 13 and 26 eV. Pathway 6 with product ion *m/z* 821.2 for $[a_3+x_3+Zn(II)]^-$ was found for all four collision energies. Pathway 7 for the loss of terminal acetyl group occurred at all energies and mostly due to shattering at 13, 26, and 39 eV. Pathway 8 with product ion *m/z* 860.2 for the loss of terminal amide group was observed mostly as a result of shattering for 10.8, 13, and 26 eV. Pathway 9 with product ion m/z 738.1 for $[y_6+Zn(II)]^-$ was observed for all four E_{rel}. Pathway 10 involved multiple bond dissociations to generate $[x_5+S+Zn(II)]^-$ with *m/z* 696.1. It was found for energies of 10.8, 13, and 26 eV.

For simulations at higher collision energies (26 and 39 eV) there are 69±5 % and 85±6 % shattering pathways, respectively. The shattering percentage is less than that for similar collision energies of TIK$(H^+)_2$[36,37] mainly because of the unavailability of the sidechains due to the tetra-coordinated zinc complex. Both thiol groups of cysteine and imidazole groups of histidine are bonded to zinc: they are less exposed to projectile and more importantly, if the collision breaks the bond with zinc, this does not always lead to a fragmentation. Since thiol side chains are bound to the zinc, the percentage of overall reactive as well as shattering trajectories is lowered with respect to a free peptide. Loss of the sidechain of the Tyr residue which is not bound to zinc (corresponding to pathway 11) is on the other hand observed for collision energies of 13 eV and higher almost exclusively as a result of a shattering mechanism. Product ion $[y_5+Zn(II)]^-$ with *m/z* 636.1, labelled pathway 12, was observed at 10.8, 13, and 39 eV. Pathway 13 was the loss of terminal methyl group which was observed for three higher energies exclusively due to shattering. Pathway 14, due to the loss of SCH_2, was observed at 13, 26, and 39 eV almost exclusively because of shattering. Product ion $[b_3+x_3+Zn(II)]^-$ with *m/z* 849.1, pathway 15, was found at 13, 26, and 39 eV. Pathway 16 involved a proton transfer from terminal carboxyl group to thiol group of Cys_7 followed by the loss of HS radical to generate product ion with *m/z* 885.2. Pathway 17 gave $[a_6+Zn(II)]^-$ ion with *m/z* 771.2 and was observed at 13, 26, and 39 eV. Loss of CO+COOH with *m/z* 845.2, shown as pathway 18 in Figure S1, was observed at 13, and 39 eV. Pathway 19 for product ion *m/z* 889.2 was observed due to the loss of CH_2NH at 26 and 39 eV. Pathway 20 (product ion *m/z* 840.2 for the loss of (H_2S+CO_2)) is observed for collision energies of 10.8 and 13 eV. The same *m/z* 840.2 is also observed due to the loss of (SCO+H_2O) at 10.8 eV but is not shown here.

In the CID of amino acids and peptides, the loss of (CO+H_2O), CO_2H_2, CO, and the iminium ion $[CH_2{=}NH_2]^+$ are a few of the most common fragmentation pathways.[67–73] All of these pathways were observed here at one or more collision energies. The loss of CO_2H_2, shown in Scheme 1, was observed at E_{rel} = 13 eV: the carboxyl group at the C-terminus picks the proton on the phenol of Tyr and then the C-C bond dissociation occurs. The loss of (CO+H_2O) was found for E_{rel} = 13 eV. Loss of CO, pathway 4 in Figure S1, is one of the most common pathways for each E_{rel}. The loss of the iminium ion is shown as pathway 19.

PCCP RSCPublishing

ARTICLE

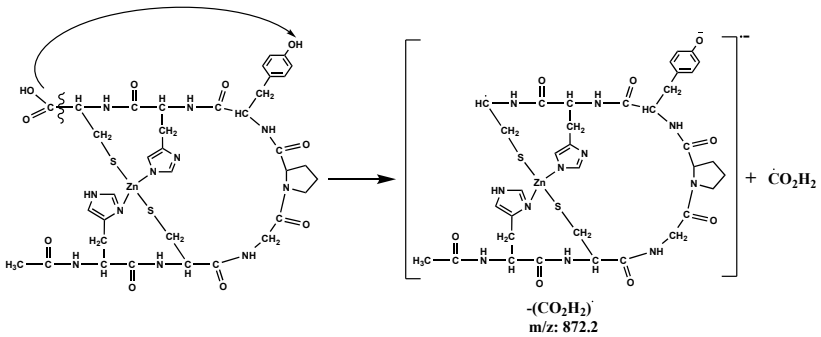

Scheme 1. Schematic diagram of formation of CO_2H_2.

Effect of Impact Parameter on Fragmentations. A previous study[36] has shown that in collision dynamics it is important to correctly set the maximum value of the randomly chosen impact parameter (b_{max}). In particular this is crucial when investigating the shattering mechanisms, since one should obtain both backbone and sidechain shattering. A very small b_{max} would disproportionately give more backbone shattering and a very large b_{max} would result in many non-reactive trajectories, with insufficient internal energy transfer, increasing the computational cost. Figure 3 shows the distributions of impact parameters versus the number of shattering trajectories for the collision dynamics simulations at E_{rel} = 13 eV.

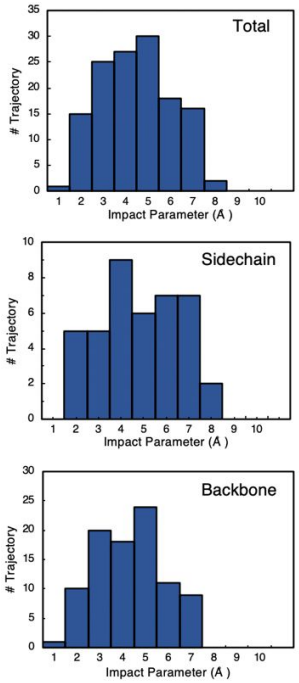

Figure 3. Distribution of impact parameter trajectories resulting in the shattering fragmentation of total, sidechain, and backbone [amb$_5$–3H+Zn(II)]$^-$ at 13 eV collision energy.

The figure shows the distributions for shattering (total, backbone and sidechain, where sidechain includes the H and H_2 loss). Table 1 lists the dissociation sites for the most important pathways. The probability of total shattering increases with b in the 2-5 Å range, while it decreases for b between 6-8 Å. Notably, only sidechain shattering is observed for $b > 7$ Å and the maximum b at which backbone shattering occurs is 7 Å. The average b for total, backbone, and sidechain shattering trajectories is 3.9, 3.8, and 4.3 Å, respectively. This result emphasizes the importance of choosing large enough b_{max} to allow proportionate backbone and sidechain shattering.

Shattering Fragmentations. As shown in Figure 4, the percentage of shattering fragmentation increases with increase in E_{rel}: from 36 ± 1 % to 85 ± 6 % when the energy increases from 10.8 to 39 eV. It is thus interesting to follow how the localization of fragmentations behaving with a shattering mechanism changes as a function of collision energy. Table 2 shows the percentage of backbone and sidechain fragmentation out of total reactive trajectories as well as the percentage of the shattering fragmentation mechanisms. Note that reactive trajectories resulting in loss of H or H_2 (which occur with a shattering mechanism) are not considered and thus the sum of backbone plus sidechain is not 100%. Similar to a previous study,[36] backbone fragmentation is more important at lower energies, in fact it goes down from 84% at 10.8 eV to 58% at 39 eV whereas sidechain fragmentation hovers around 20% for 13-39 eV and is only 11% for 10.8 eV. Percentage of backbone shattering trajectories goes from 64% to 74% when energy is increased from 10.8 to 13 eV but goes down to 49% and 52% for 26 and 39 eV primarily due to the fact that these percentages do not include the fragmentation due to the loss of H atom or H_2 molecule both of which are exclusively due to shattering. The loss of H and H_2 comprise 5%, 10%, 18% and 21% of total reactive trajectories for energies of 10.8, 13, 26, and 39 eV, respectively.

Table 2. Percentages of backbone and sidechain dissociation and shattering fragmentation

	% fragmentation[a]		% shattering[b]	
E_{rel} (eV)	Backbone	Sidechain	Backbone	Sidechain
10.8	84 ± 3	11 ± 2	64 ± 1	23 ± 2
13	71 ± 4	19 ± 4	74 ± 3	23 ± 3
26	60 ± 3	22 ± 2	49 ± 3	25 ± 2
39	58 ± 3	21 ± 4	52 ± 3	24 ± 4

[a] *Percentage of backbone and sidechain fragmentation out of the total reactive trajectories.* [b] *Percentage of total reactive trajectories that are shattering excluding hydrogen atom/molecule loss. The standard deviation of the percentage is also provided.*

Energy Transfer. In addition to providing information about the fragmentation products and mechanisms, collision activated simulations can also provide the energy transferred to the internal energy of the ion. Figure S2 shows the distribution of change in internal energies in kcal/mol versus the number of trajectories for all the collision energies. Table 3 lists the summarized properties of the energy transfer to the internal energy of $[amb_5–3H+Zn(II)]^-$ at different collision energies. In each case, the average energy for the reactive trajectories ($\langle E\rangle_{react}$) is way higher than that of non-reactive trajectories ($\langle E\rangle_{non\text{-}react}$). We can obtain, for each E_{rel}, the minimum energy value for which a fragmentation is observed, E_{min} (Table 3). We can thus define $P(E > E_{min})$ as the percentage of non-reactive trajectories with transferred energy greater than E_{min}. The high values of $P(E > E_{min})$, which varies from 27-36% for different E_{rel}, and minimum fragmentation energies is also due to the fact that the non-reactive trajectories include those that undergo a proton transfer or one or more bond dissociations without generating two or more fragments.

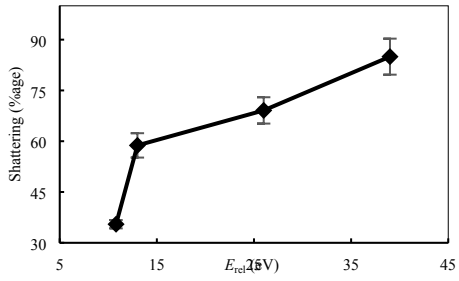

Figure 4. Percentage of shattering trajectories with respect to the total reactive trajectories versus relative translational energy (eV). The error bars show one standard deviation.

Table 3. Summarized energy transfer properties for CID of $[amb_5–3H+Zn(II)]^-$[a]

E_{rel} (eV)	10.8	13	26	39
$\langle E\rangle_{react}$	193 ± 25	229 ± 35	397 ± 99	469 ±177
$\langle E\rangle_{non\text{-}react}$	58 ± 66	67 ± 82	56 ± 93	82 ± 128
E_{min}	115.4	126.6	121.5	134.2
$P(E > E_{min})$	35%	36%	29%	27%
$\langle E\rangle_{shattering}$	199 ± 26	228 ± 44	372 ± 109	467 ± 171
$E^{min}_{shattering}$	127.4	129.4	118.9	136.5

[a] *E_{rel} is in eV and all the other energies in kcal/mol. $\langle E\rangle_{react}$ is the average energy transferred for reactive trajectories. $\langle E\rangle_{non\text{-}react}$ is the average transferred energy for non-reactive trajectories. E_{min} is the minimum energy required to undergo dissociation. $P(E > E_{min})$ is the percentage of non-reactive trajectories with internal energy transfer greater than E_{min}. $\langle E\rangle_{shattering}$ is the average transferred energy for shattering trajectories. $E^{min}_{shattering}$ is the minimum energy required for shattering. The reported uncertainties are one standard deviation*

In our previous work,[61] Arrhenius activation energies were calculated from direct dynamics simulations of thermally excited $[amb_5–3H+Zn(II)]^-$. Following the statistical redistribution of the ion's vibrational energy and RRKM unimolecular kinetics, the minimum activation energy was found to be 35.8 kcal/mol for pathway 1. From the analysis of non-shattering trajectories, we found a minimum value which is substantially higher, notably: 115.4 kcal/mol. In CID, non-shattering trajectories should follow statistical fragmentation when they are run for longer times. Here, the trajectories were integrated for a short time of 20ps, hence, non-shattering trajectories do not correspond to the thermal statistical limit of 35.8 kcal/mol. In other words, non-reactive trajectories with energy transferred less than 115.4 kcal/mol during CID may react if they are run on longer time scales, which is computationally unaffordable for $[amb_5–3H+Zn(II)]^-$. On the other hand, our simulation time is long enough for an accurate study of shattering trajectories.

The minimum energy threshold for shattering of $[amb_5–3H+Zn(II)]^-$ is 118.9 kcal/mol, as also reported in Table 3. Since sidechains of cysteine and histidine are bound to Zn(II), when they break right after collision with Ar, this will not lead to a direct fragmentation. This reduces considerably the shattering probability and increases the shattering threshold. The nature of the complex also reduces the number of hydrogen atoms exposed to the projectile. The unavailability of the side chains is probably another reason that no reactive trajectories were observed at collision energies lower than 10.8 eV.

The shattering threshold of 118.9 kcal/mol is substantially higher than the lowest threshold of 35.8 kcal/mol obtained during the thermal dissociation[61] of $[amb_5–3H+Zn(II)]^-$. It reaffirms the previous finding[37] that due to the higher energies required for shattering as compared to the statistical fragmentation, the former may not play a big role in determining fragmentation products in threshold-CID experiments.

Thermal versus CID Fragmentation of $[amb_5–3H+Zn(II)]^-$. In this section, the relevant fragment ions for collisional and thermal simulations are compared. In previous studies[36,38] it has been discussed that both statistical (thermal fragmentation) and non-statistical (single collision simulations) mechanisms contribute to the peaks observed in an experimental mass spectrum. All dissociations in thermal excitation simulations are by definition non-shattering whereas in CID simulations both shattering and non-shattering fragmentation can occur.

Table 4 reports the results for the most abundant product ions obtained in thermal simulations to be compared with collisional simulation results summarized in Table 1. In particular, for collisional simulations we discuss the percentages of shattering *vs* non-shattering mechanisms from Table 1 for E_{rel} = 10.8 and 13 eV. Here we describe in detail the different behaviours.

The ion $[x_6+Zn(II)]^-$, *m/z* 766.1 corresponding to pathway 1 in Figure S1, was one of the most abundant ions for thermal excitation and it was also found for all the E_{rel} during CID simulations. It was not observed for the highest temperature of 2250 K because at this high temperature the ion further dissociated to give other fragmentations. During CID its percentage was 21% for 10.8 eV but remained around

7% for higher collision energies mainly because of the increased number of pathways. At the lowest collision energy of 10.8 eV it occurred almost exclusively due to non-shattering mechanism whereas at 13 eV one third was due to shattering. Ion *m/z* 873.2 (pathway 2) was due to the loss of C-terminus carboxylate group, COOH, which was observed for all temperatures. About two thirds of this pathway occurred due to shattering even at the lower collision energies of 10.8 and 13 eV. Ion *m/z* 837.2 (pathway 3), loss of CH_2+imidazole, was found for the four highest temperatures and for all the collision energies. 75% of this pathway happened due to shattering at 10.8 eV. Pathway 4, product ion *m/z* 890.2, corresponding to the loss of CO molecule, happens mostly with shattering except at 10.8 eV at which 60% happens due to non-shattering mechanism. Loss of CO molecule was observed at all temperatures during thermally excited fragmentations. Ion *m/z* 723.1 ($[z_6+Zn(II)]^-$ in pathway 5) was found for all the temperatures and collision energies. 50% of the times it occurred due to shattering at both 10.8 and 13 eV collision energies. Pathway 6 (ion *m/z* 821.2 with fragment $[a_3+x_3+Zn(II)]^-$) happened mostly due to non-shattering mechanism and it is also observed at four temperatures in thermal simulations. Ion with *m/z* 875.2 could refer to the loss of either one of CONH molecule or $COCH_3$. Here, as shown in pathway 7, it corresponded to the loss of $COCH_3$ molecule. It was found for the four higher temperatures and all the collision energies and happened mostly due to non-shattering in CID simulations. Ion with *m/z* 738.1 (fragment $[y_6+Zn(II)]^-$ in pathway 9) was observed for two highest temperatures and all the collision energies and occurred due to shattering at 10.8 eV and mostly non-shattering at 13 eV. Pathway 12 (ion $[y_5+Zn(II)]^-$, *m/z* 636.1) involved breaking of three bonds and happened mostly because of non-shattering mechanism as expected. The fragmentation of the small molecules and sidechains exposed to the projectile happened mostly due to shattering as compared to the other parts of the ion.

Table 4. Relative abundances of dominant fragment ions for thermal simulations.

	Thermal Simulation Temperature[a] (K)				
m/z	1600	1750	1875	2000	2250
766.1	100.0	100.0	73.3	100.0	-
873.2	14.3	19.0	100.0	58.0	40.0
837.2	-	19.0	40.0	17.0	40.0
738.1	-	-	-	42.0	40.0
723.1	14.3	9.5	46.6	100.0	100.0
821.2		19.0	20.0	25.0	20.0
890.2	42.8	9.5	60.0	17.0	60.0
875.2	42.8	4.8	66.6	42.0	-
636.1	-	-	-	-	40.0

[a] *Results from ref. 51 for conformer a of* $[amb_5–3H+Zn(II)]^-$.

Fragmentation Ions Unique of CID Simulations and Experiments. Detailed comparison between the results of thermal simulations of three conformers of $[amb_5–3H+Zn(II)]^-$ and the experiment[6] has been performed in a previous work[61] and a comparison of thermal and CID simulation results has been performed in previous section. Here, we discuss only two product ions which are unique in collisional simulations with respect to experiments (as in Ref 51), namely *m/z* 885.2 and 840.2. Ion *m/z* 885.2 (pathway 16) corresponded to the loss of SH radical and was observed for collision energies 13 eV and higher. The experiment found *m/z* 884.2 corresponding to the loss of H_2S molecule. This pathway was not observed in simulations, probably because one needed a second H-transfer to sulfur atom, not observed in simulation time. In simulations, loss of H_2S is observed only with loss of a second neutral, CO_2. This led to ion *m/z* 840.2 which was the second product ion observed in collisional simulations and not in thermal ones. This ion was observed in experiments and attributed to $CO_2 + H_2S$ or $SCO + H_2O$ loss. Interestingly, both these mechanisms were observed for CID simulations: at 13 eV we observed loss of $CO_2 + H_2S$, while at 10.8 eV loss of $SCO + H_2O$. This supported the experiment that both neutral losses are possible.

Conclusions

In this article, we report chemical dynamics simulations of collisions between a Zn(II) containing oligopeptide (acetyl-His_1-Cys_2-Gly_3-Pro_4-Tyr_5-His_6-Cys_7 labelled here $[amb_5–3H+Zn(II)]^-$) and Ar atom at different energies. From simulations, we obtained and studied in detail the fragmentation products and their corresponding mechanisms. The results are compared with previous thermal simulations[61] as well as multiple collision ion mobility MS/MS experimental spectrum.[6] The collisional simulations are able to provide details on the first pico-seconds subsequent to the collision with Ar.

The collisional and thermal simulations show similar product ions with differences in some abundances and mechanisms. This is due to the fact that in collision induced dissociation there is both statistical and non-statistical fragmentation as compared to only statistical dissociation in thermal excitation. In particular, we have analysed carefully the so-called shattering fragmentations, which are characteristic examples of non-statistical fragmentation and which can occur in CID simulations and not in thermal ones by definition.

From the energy transfer analysis, we obtained that the minimum energy required to undergo shattering is 118.9 kcal/mol which is substantially higher than the Arrhenius activation barrier of 35.8 kcal/mol found using direct dynamics of statistical thermal fragmentations.[61] Note that in a previous work on a linear peptide we have also found that the shattering threshold is higher than the Arrhenius barrier (55 vs 15 kcal/mol, respectively). Remarkably, the shattering threshold is in both cases about three times higher than Arrhenius activation energy.

The tetrahedral nature of the zinc complex determines the fragmentation mechanisms of CID simulations. The unavailability of sidechains of both cysteine and histidine due to covalent bonding with Zn(II), results in higher collision energy needed for fragmentation and increased internal energy transfer to undergo either backbone or sidechain dissociation with respect to what observed in similar free peptides.[36,37,55,74] Note that, in most of the pathways, due to the tetra-coordinated Zn(II) complex, two or more bonds must be broken to generate fragments. When Ar atom hits on cysteine or histidine sidechains it can break a bond but without any resulting fragment. To obtain a fragment a second bond must be broken, which can happen after that the energy flows through the molecule. This by definition does no correspond anymore to a shattering mechanism. The nature of the complex also reduces the number of hydrogen atoms exposed to the projectile making them less susceptible to undergo shattering.

For these reasons there are no reactive trajectories below E_{rel} = 10.8 eV and the minimum energy required for shattering is 118.9 kcal/mol. Furthermore, the threshold for non-shattering fragmentations is also high (115.4 kcal/mol, only 3.5 kcal/mol lower than the shattering one). This can be due to the limited simulation time not allowing for enough efficient intramolecular vibrational energy redistribution. For this

reason, thermal simulations provide a more accurate description of statistical fragmentations, which is complementary to the present one.

In conclusion, the tetra-coordinated nature of the zinc complex guides the CID simulations. Since the sidechains of both cysteine and histidine are covalently bound to zinc, they are not readily available to dissociate. This not only results in higher collision energy required to achieve fragmentation but also increases the internal energy transferred to have either backbone or sidechain dissociations. The tetra-coordinated complex also implies that not every bond dissociation ends up in fragmentation with most of the pathways reported requiring at least two or more bonds to be broken to generate fragments.

Acknowledgments

The research at Texas Tech University (TTU) was supported by the Robert A. Welch Foundation under Grant No. D-0005. The research at Texas A&M-Commerce was supported by the National Science Foundation under grant 1764436, and the Welch Foundation (T-0014). The simulations were performed with the computer clusters Chemdynm of the Hase Research Group and Quanah of the TTU High Performance Computing Center. The authors would like to dedicate this work to the memory of Prof. W.L. Hase, who passed away too soon few days before the submission of this work.

Conflicts of interest

Authors declare no conflict of interest in this work.

References

1 C. A. Blindauer, *J. Inorg. Biochem.*, 2013, **121**, 145–155.
2 A. Klug, *Annu. Rev. Biochem.*, 2010, **79**, 213–231.
3 L. Banci, I. Bertini, S. Ciofi-Baffoni, L. A. Finney, C. E. Outten and T. V O'Halloran, *J. Mol. Biol.*, 2002, **323**, 883–897.
4 I. Sóvágó, C. Kállay and K. Várnagy, *Coord. Chem. Rev.*, 2012, **256**, 2225–2233.
5 I. Sóvágó, K. Várnagy, N. Lihi and Á. Grenács, *Coord. Chem. Rev.*, 2016, **327–328**, 43–54.
6 S. M. Wagoner, M. Deeconda, K. L. Cumpian, R. Ortiz, S. Chinthala and L. A. Angel, *J. Mass Spectrom.*, 2016, **51**, 1120–1129.
7 T. Dudev and C. Lim, *Chem. Rev.*, 2014, **114**, 538–556.
8 M. Whittaker, C. D. Floyd, P. Brown and A. J. H. Gearing, *Chem. Rev.*, 1999, **99**, 2735–2776.
9 C. Gialeli, A. D. Theocharis and N. K. Karamanos, *FEBS J.*, 2011, **278**, 16–27.
10 A. Klug, *Q. Rev. Biophys.*, 2010, **43**, 1–21.
11 K. L. Chan, I. Bakman, A. R. Marts, Y. Batir, T. L. Dowd, D. L. Tierney and B. R. Gibney, *Inorg. Chem.*, 2014, **53**, 6309–6320.
12 A. Nomura and Y. Sugiura, *Inorg. Chem.*, 2002, **41**, 3693–3698.
13 S. S. Krishna, I. Majumdar and N. V Grishin, *Nucleic Acids Res.*, 2003, **31**, 532–550.
14 E. N. Yousef and L. A. Angel, *J. Mass Spectrom.*, 2020, **55**, e4489.
15 Y.-F. Lin, E. N. Yousef, E. Torres, L. Truong, J. M. Zahnow, C. B. Donald, Y. Qin and L. A. Angel, *J. Am. Soc. Mass Spectrom.*, 2019, **30**, 2068–2081.
16 D. Choi, R. Sesham, Y. Kim and L. A. Angel, *Eur. J. Mass Spectrom.*, 2012, **18**, 509–520.
17 J. W. McCabe, R. Vangala and L. A. Angel, *J. Am. Soc. Mass Spectrom.*, 2017, **28**, 2588–2601.
18 R. Sesham, D. Choi, A. Balaji, S. Cheruku, C. Ravichetti, A. A. Alshahrani, M. Nasani and L. A. Angel, *Eur. J. Mass Spectrom.*, 2013, **19**, 463–473.
19 D. Choi, A. A. Alshahrani, Y. Vytla, M. Deeconda, V. J. Serna, R. F. Saenz and L. A. Angel, *J. Mass Spectrom.*, 2015, **50**, 316–325.
20 Y. Vytla and L. A. Angel, *Anal. Chem.*, 2016, **88**, 10925–10932.
21 E. N. Yousef, R. Sesham, J. W. McCabe, R. Vangala and L. A. Angel, *JoVE*, 2019, e60102.
22 J. S. Brodbelt, *Anal. Chem.*, 2016.
23 S. A. McLuckey, *J. Am. Soc. Mass Spectrom.*, 1992, **3**, 599–614.
24 S. Pratihar, X. Ma, Z. Homayoon, G. L. Barnes and W. L. Hase, *J. Am. Chem. Soc.*, 2017, **139**, 3570–3590.
25 A. Martin Somer, V. Macaluso, G. L. Barnes, L. Yang, S. Pratihar, K. Song, W. L. Hase and R. Spezia, *J. Am. Soc. Mass Spectrom.*, 2020, **31**, 2–24.
26 J. Laskin and J. H. Futrell, *Mass Spectrom. Rev.*, 2003, **22**, 158–181.
27 A. G. Harrison, *Mass Spectrom. Rev.*, 2009, **28**, 640–654.
28 T. Yalcin, I. G. Csizmadia, M. R. Peterson and A. G. Harrison, *J. Am. Soc. Mass Spectrom.*, 1996, **7**, 233–242.
29 B. Paizs and S. Suhai, *Mass Spectrom. Rev.*, 2005, **24**, 508–548.
30 L. J. M. Kempkes, J. Martens, J. Grzetic, G. Berden and J. Oomens, *J. Am. Soc. Mass Spectrom.*, 2016, **27**, 1855–1869.
31 A. C. Gucinski, J. Chamot-Rooke, E. Nicol, Á. Somogyi and V. H. Wysocki, *J. Phys. Chem. A*, 2012, **116**, 4296–4304.
32 R. N. Grewal, H. El Aribi, A. G. Harrison, K. W. M. Siu and A. C. Hopkinson, *J. Phys. Chem. B*, 2004, **108**, 4899–4908.
33 J. Grzetic and J. Oomens, *J. Am. Soc. Mass Spectrom.*, 2013, **24**, 1228–1241.
34 C. R. Nelson, M. T. Abutokaikah, A. G. Harrison and B. J. Bythell, *J. Am. Soc. Mass Spectrom.*, 2016, **27**, 487–497.
35 I. Komáromi, Á. Somogyi and V. H. Wysocki, *Int. J. Mass Spectrom.*, 2005, **241**, 315–323.
36 Z. Homayoon, V. Macaluso, A. Martin-Somer, M. C. N. B. Muniz, I. Borges, W. L. Hase and R. Spezia, *Phys. Chem. Chem. Phys.*, 2018, **20**, 3614–3629.
37 V. Macaluso, Z. Homayoon, R. Spezia and W. L. Hase, *Phys. Chem. Chem. Phys.*, 2018, **20**, 19744–19749.
38 R. Spezia, A. Martin-Somer, V. Macaluso, Z. Homayoon, S. Pratihar and W. L. Hase, *Faraday Discuss.*, 2016, **195**, 599–618.
39 A. Martin-Somer, R. Spezia and M. Yáñez, *Philos. Trans. R. Soc. A Math. Phys. Eng. Sci.*, ,

DOI:10.1098/rsta.2016.0196.

40 I. A. Papayannopoulos, *Mass Spectrom. Rev.*, 1995, **14**, 49–73.

41 E. Uggerud and P. J. Derrick, *J. Phys. Chem.*, 1991, **95**, 1430–1436.

42 K. Park, B. Deb, K. Song and W. L. Hase, *J. Am. Soc. Mass Spectrom.*, 2009, **20**, 939–948.

43 S. O. Meroueh, Y. Wang and W. L. Hase, *J. Phys. Chem. A*, 2002, **106**, 9983–9992.

44 S. Pratihar, G. L. Barnes and W. L. Hase, *Chem. Soc. Rev.*, 2016, **45**, 3595–3608.

45 O. Meroueh and W. L. Hase, *Phys. Chem. Chem. Phys.*, 2001, **3**, 2306–2314.

46 J. Laskin, T. H. Bailey and J. H. Futrell, *J. Am. Chem. Soc.*, 2003, **125**, 1625–1632.

47 S. Pratihar, G. L. Barnes, J. Laskin and W. L. Hase, *J. Phys. Chem. Lett.*, 2016, **7**, 3142–3150.

48 W. L. Baer, T.; Hase, *Unimolecular Reaction Dynamics. Theory and Experiments*, Oxford, New York, 1996.

49 R. Spezia, J.-Y. Salpin, M.-P. Gaigeot, W. L. Hase and K. Song, *J. Phys. Chem. A*, 2009, **113**, 13853–13862.

50 T. Yan and W. L. Hase, *Phys. Chem. Chem. Phys.*, 2000, **2**, 901–910.

51 Y. Jeanvoine, M.-P. Gaigeot, W. L. Hase, K. Song and R. Spezia, *Int. J. Mass Spectrom.*, 2011, **308**, 289–298.

52 E. Rossich Molina, J.-Y. Salpin, R. Spezia and E. Martínez-Núñez, *Phys. Chem. Chem. Phys.*, 2016, **18**, 14980–14990.

53 E. R. Molina, D. Ortiz, J.-Y. Salpin and R. Spezia, *J. Mass Spectrom.*, 2015, **50**, 1340–1351.

54 E. Martínez-Núñez, S. A. Vázquez and J. M. C. Marques, *J. Chem. Phys.*, 2004, **121**, 2571–2577.

55 C.-Y. Ng, *J. Phys. Chem. A*, 2002, **106**, 5953–5966.

56 E. Martínez-Núñez, A. Fernández-Ramos, S. A. Vázquez, J. M. C. Marques, M. Xue and W. L. Hase, *J. Chem. Phys.*, 2005, **123**, 154311.

57 R. Spezia, J. Martens, J. Oomens and K. Song, *Int. J. Mass Spectrom.*, 2015, **388**, 40–52.

58 R. Spezia, S. B. Lee, A. Cho and K. Song, *Int. J. Mass Spectrom.*, 2015, **392**, 125–138.

59 K. I. M. Bolton, W. L. Hase and G. H. Peslherbe, in *Modern Methods for Multidimensional Dynamics Computations in Chemistry*, WORLD SCIENTIFIC, 1998, pp. 143–189.

60 L. Sun and W. L. Hase, in *Reviews in Computational Chemistry*, John Wiley & Sons, Ltd, 2003, pp. 79–146.

61 A. Malik, Y.-F. Lin, S. Pratihar, L. Angel and W. Hase, *J. Phys. Chem. A*, 2019, **123**, 6868–6885.

62 J. J. P. Stewart, *J. Mol. Model.*, 2013, **19**, 1–32.

63 X. Hu, W. L. Hase and T. Pirraglia, *J. Comput. Chem.*, 1991, **12**, 1014–1024.

64 J. P. Stewart, 2012.

65 G. H. Peslherbe, H. Wang and W. L. Hase, *Adv. Chem. Phys.*, 1999, 171–201.

66 P. Roepstorff and J. Fohlman, *Biomed. Mass Spectrom.*, 1984, **11**, 601.

67 S. Abirami, Y. M. Xing, C. W. Tsang and N. L. Ma, *J. Phys. Chem. A*, 2005, **109**, 500–506.

68 K. Zhang, D. M. Zimmerman, A. Chung-Phillips and C. J. Cassady, *J. Am. Chem. Soc.*, 2002, **115**, 10812–10822.

69 H. El Aribi, G. Orlova, C. F. Rodriquez, D. R. P. Almeida, A. C. Hopkinson and K. W. Michael Siu, *J. Phys. Chem. B*, 2004, **108**, 18743–18749.

70 R. A. J. O'Hair, P. S. Broughton, M. L. Styles, B. T. Frink and C. M. Hadad, *J. Am. Soc. Mass Spectrom.*, 2000, **11**, 687–696.

71 J. Laskin, E. Denisov and J. Futrell, *J. Am. Chem. Soc.*, 2000, **122**, 9703–9714.

72 S. Beranova, J. Cai and C. Wesdemiotis, *J. Am. Chem. Soc.*, 2002, **117**, 9492–9501.

73 C. W. Tsang and A. G. Harrison, *J. Am. Chem. Soc.*, 2002, **98**, 1301–1308.

74 K. Song, S. Meroueh and W. L. Hase, *J. Chem. Phys.*, 2003, **118**, 2893–2902.